Relationship between Euler buckling and unstable equilibria of buckled beams

Mihaela Nistor[a], Richard Wiebe[b], Ilinca Stanciulescu[a,*]

[a] *Rice University, Department of Civil and Environmental Engineering, 6100 Main Street, Houston, TX, 77005, U.S.A*

[b] *University of Washington, Department of Civil and Environmental Engineering, 201 More Hall, Box 352700, Seattle, WA, U.S.A.*

Abstract

Classic snap-through of curved beams, plates, and shells has long been an object of attention in structural engineering. Euler buckling under axial loading is perhaps an even more entrenched part of the canon of engineering education and practice. In this paper we introduce a relationship between the two phenomena, that to our knowledge has not been directly addressed before. The relationship shows that Euler buckling configurations are connected by the force-displacement curve under transverse loading. The results are used to develop a very simple metric to estimate the number of unstable static equilibria of a buckled structure based only on its geometry with no need for static or dynamic solvers. The study is focused on beams as this allows for an unambiguous discussion of the idea on the simplest possible structure.

Keywords: snap-through, Euler buckling, stability, arc-length method, structural mechanics

---

*Corresponding author. Tel.: +1713 348 4704; fax: +1713 348 5268.
Email address: ilinca.s@rice.edu (Ilinca Stanciulescu)

1. Background and Motivation

Static and dynamic snap-through of curved structures such as beams and plates is the subject of much research in the literature [1–8], to the extent that it was the main driving force in the initial development of the arc-length method [9, 10]. This is not surprising, as it has proven to be an important critical phenomenon, for example in slender aerospace structures [11, 12]. Alternatively, it is sometimes seen as a desirable phenomenon in switching [13–16], filtering [17], and energy harvesting applications [18].

Despite the long history of research, snap-through continues to yield new and surprising results. This is particularly true for continuous (infinite dimensional) systems such as beams or plates, as they may present extremely complex potential energy hyper-surfaces with the possibility for bifurcations under both axial and transverse loading, or under changes of geometric parameters. For example, in [19] it was shown, using arc-length path following of equilibrium solutions [10] and branch-switching [20, 21], that curved structures may exhibit many "hidden" unstable equilibrium curves that emanate out of a series of critical point bifurcations.

In this paper, we present a connection between the Euler buckling loads for initially flat beams and the force-displacement curve under transverse loading for buckled beams. Through this connection, a simple calculation provides insight into the degree of instability (the number of unstable equilibria) of beams without running any simulations.

The driving idea behind the paper is illustrated in Fig. 1. Part (a) shows a schematic of an initially flat beam, buckled well beyond the first Euler buckling load (which could be caused by thermal load, or displacement of the supports) and subsequently subjected to a transverse point load applied at an offset from the middle. The corresponding force-displacement curve obtained via arc-length path following is shown in part (b). Also illustrated in part (b) are the configurations of the structure at the zero-transverse-load crossings (ZTLCs) (locations marked with circles where the transverse force is equal to zero on the equilibrium curve). The equilibrium configurations labeled 1, 2, 4, and 5 are very similar to the classic Euler buckling mode shapes.

Although only three ZTLCs are marked (Fig. 1b) on the force-displacement curve, five zero load crossings exist as the deformed shapes of the beam indicate. It appears as if at the middle zero load crossing the curve intersects itself. This is not the case, however, as the apparent intersection is due to the projection of a high-dimensional curve into a 2D space.

The force-displacement curve can be qualitatively described by the number of ZTLCs, or by the number of "loops" it makes before reaching the snapped-through stable equilibrium (state 5 in Fig. 1). Additional "loops" in the force-displacement curve, and therefore additional zero crossings (and higher buckling mode shapes), can be induced by increasing the axial stiffness or by increasing the buckling-induced rise (the reason for this will be discussed later). The importance of the slight offset in the point load will also be discussed later.

In the following work we test the hypothesis that as the buckling-induced rise is reduced, the unstable zero transverse load equilibrium configurations approach the shape of the Euler buckling modes (i.e., the error between the Euler mode shapes and the unstable equilibrium configuration at the ZTLCs such as states 2 and 4 will approach zero). However, as the buckling-induced rise is reduced, the axial stiffness must be increased in order to yield higher buckling modes. The work is focused on post-buckled initially

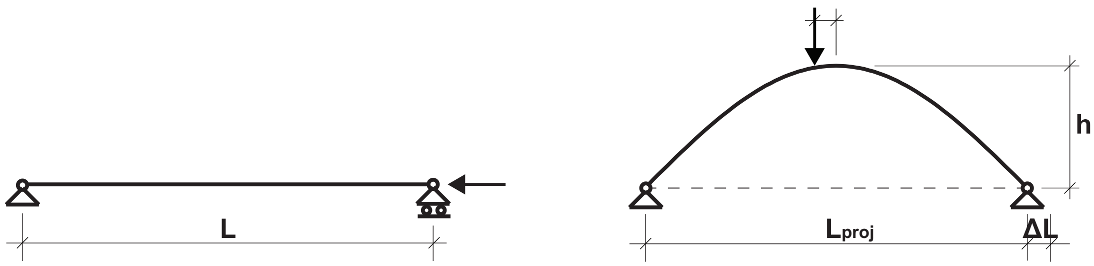

(a) Initially flat beam buckled to desired rise h and thereafter subject to transverse load.

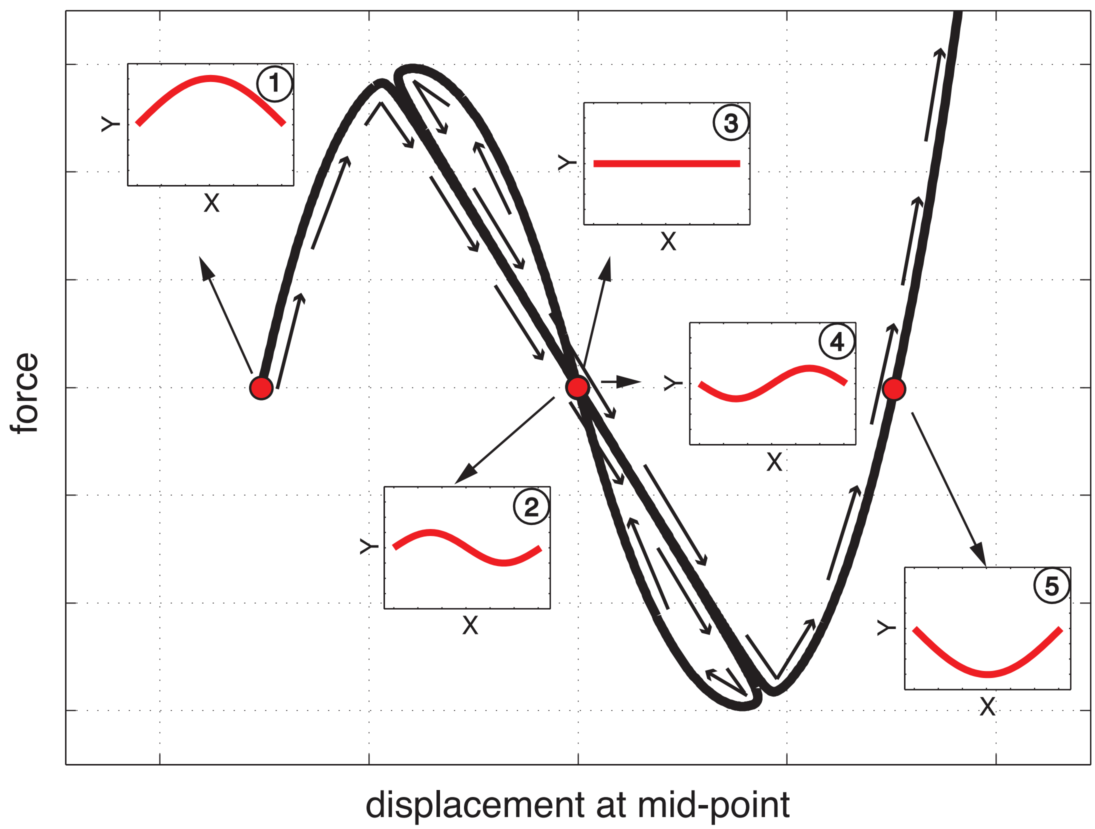

(b) Force-deflection curve with ZTLCs (red circles) and beam deformed shape at each crossing.

Figure 1: Schematics of the loading for an initially flat beam and of the transverse force-displacement curve with beam deformed shapes at ZTLCs.

flat beams without imperfections. This was intentionally done in order to allow for an exact comparison with classical Euler buckling, as imperfections or initially curved beams induce geometric bias into the system. The results, however, hold nominally for shallow curved beams, but such systems are not the focus of this paper.

The remainder of the paper is structured as follows. Section 2 introduces the connection between the Euler buckling loads and the force-displacement curve under transverse load through simple examples, and provides the estimate on the upper bound on the number of ZTLCs. Section 3 discusses the influence of geometric parameters (rise, thickness, cross-sectional area) and the effect of transverse load location and type on the equilibrium configurations and implicitly on the upper bound. Finally, Section 4 summarizes main conclusions and potential applications.

2. Connection between Euler buckling and snap-through buckling

Post-buckled initially flat beams allow for an exact comparison with the classical Euler buckling loads and mode shapes. Using the finite element method (FEM), we analyze an initially flat beam that is axially compressed until it buckles to a certain buckling level (rise) and then subjected to a transverse point load (at the center or just off-center). Pinned-pinned boundary conditions are considered. In the FEM simulations presented in this paper, we use a beam formulation based on the Euler-Bernoulli theory extended to large deformations [22]. The numerical procedure that combines arc-length and branch switching methods introduced in [23] is used to obtain the bifurcated equilibrium states using FEA.

The beam is homogeneous with Young's modulus E, length L, uniform cross-section A, moment of inertia I, Poisson's ratio ν and density ρ. These geometric and material properties are listed in Table 1.

Length (L) [mm]	304.8
Cross-section area (A) [mm^2]	0.32258
Moment of Inertia (I) [mm^4]	0.1387438
Young's Modulus (E) [N/mm^2]	206843
Poisson's Ratio (ν)	0.28
Density (ρ) [N s^2/mm^4]	7.834×10^{-9}

Table 1: Flat beam dimensions and material properties

2.1. Description via simple examples

To illustrate the relationship, consider the examples of initially flat buckled beams with transverse point load applied at the center or just off-center. In both cases the initially flat beam is first buckled to a rise $h = 3$ mm. The numerical procedure presented in [19] is used to trace the equilibrium paths under transverse force.

First we analyze the example with load applied at the center. The force-deflection curve has a primary path and two mirror image (of each other) bifurcated branches. The equilibrium path for the beam can follow either only the primary equilibrium path (black line in Fig. 2a) or it can initially begin on the primary equilibrium path, switch to one of the bifurcated branches and then return on the primary path (black line in Fig. 3a). The relationship between the axial and the transverse force at the equilibrium states is denoted by the black line in Fig. 2b and Fig. 3b respectively. We will refer to these representations as axial equilibrium plots in the remainder of the paper. In these figures, the gray lines correspond to equilibrium configurations that are not visited under the load path followed. The axial equilibrium plots also highlight why the bifurcated branches

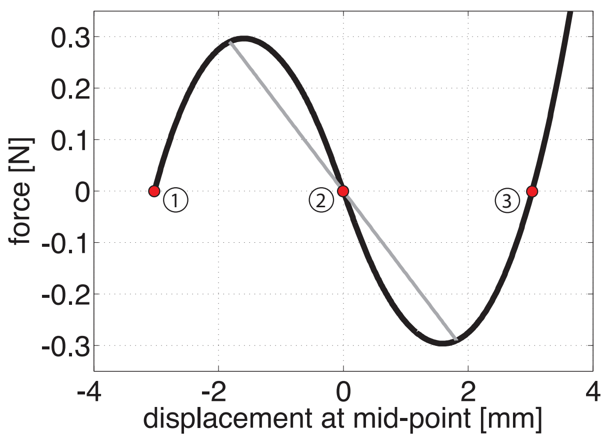

(a) Equilibribium path

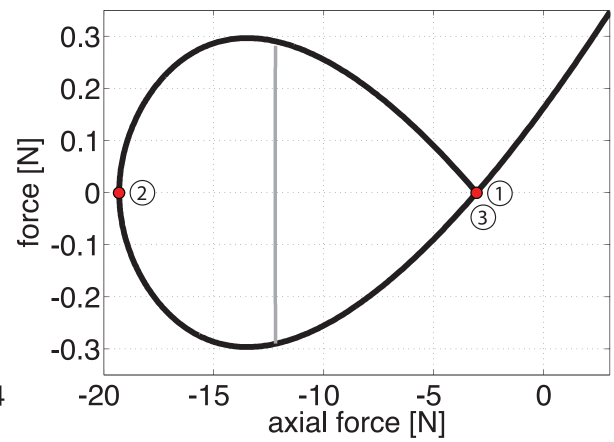

(b) Axial force

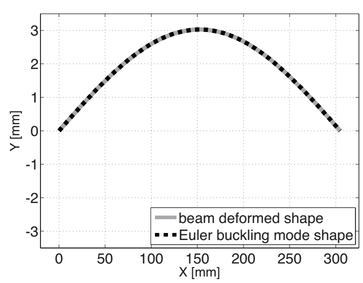

(c) Crossing 1

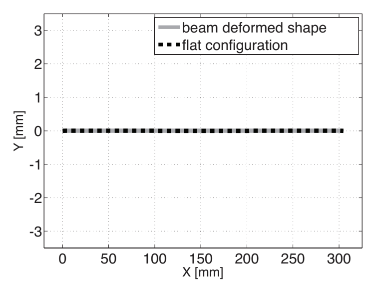

(d) Crossing 2

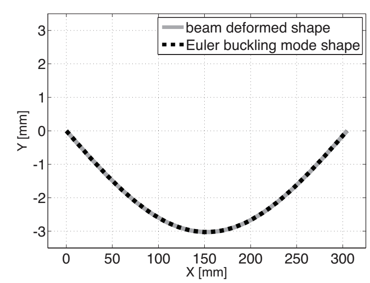

(e) Crossing 3

Figure 2: Equilibrium path and axial force for beam buckled to rise = 3 mm subject to transverse mid-point load (— Equilibrium path followed in simulation, — Equilibrium path not followed in simulation), and the beam deformed shapes at the ZTLCs compared to the Euler buckling mode shapes and the flat configuration.

are typically preferred by structures in displacement-controlled experiments (experiments inherently have imperfections), in that they have a significantly lower axial force and thereby present a lower potential energy barrier.

The ZTLCs are marked with circles in Figs. 2a and 3a. The deformed shapes of the beam at these crossings correspond to Euler buckling mode shapes or to the flat configuration (see Figs. 2c-2e and Figs. 3c-3e which show that the deformed shapes are nominally identical to the Euler buckling mode shapes). Also the axial forces in the beam

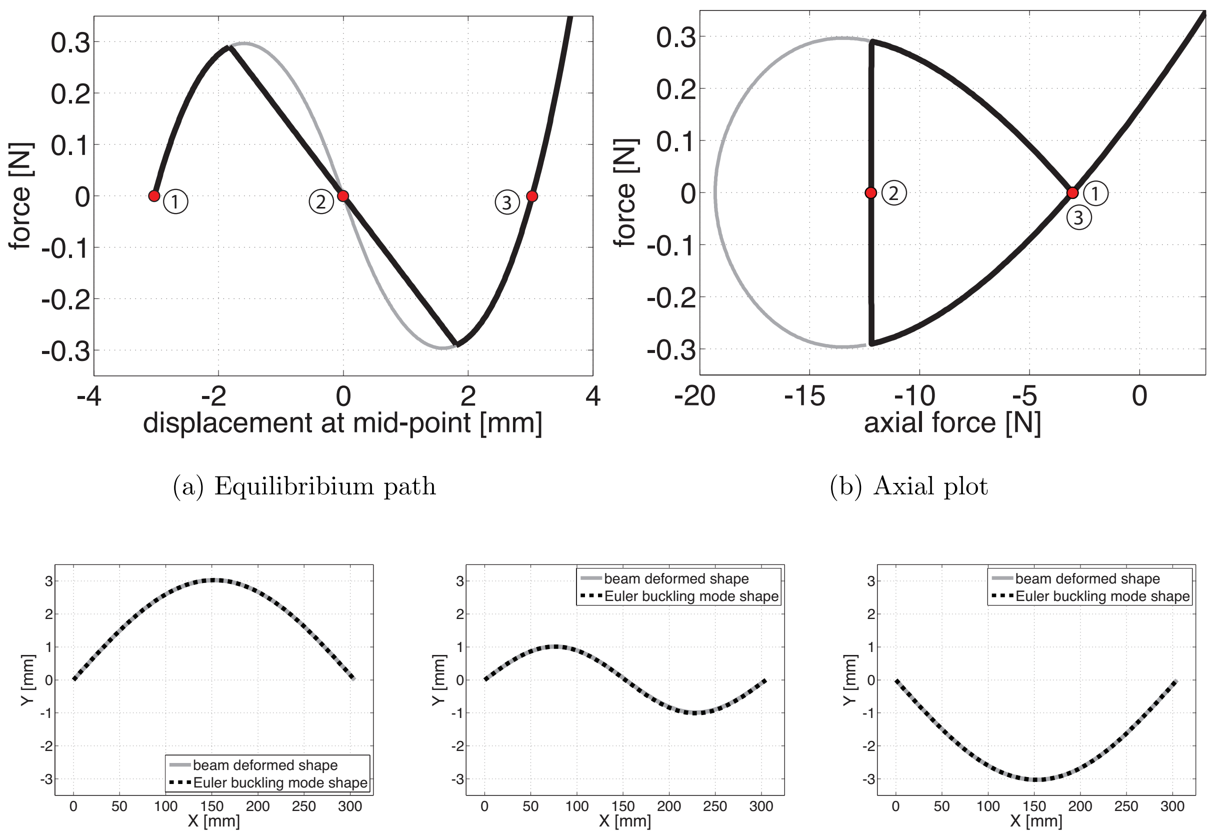

(a) Equilibribium path

(b) Axial plot

(c) Crossing 1

(d) Crossing 2

(e) Crossing 3

Figure 3: Equilibrium path (with branch switching) and axial plot for beam buckled to rise = 3 mm subject to transverse mid-point load (— Equilibrium path followed in simulation, — Equilibrium path not followed in simulation), and the beam deformed shapes at the ZTLCs compared to the Euler buckling mode shapes. Note that a mirror image of part (d) could also be visited.

correspond to the Euler buckling loads (Figs. 2c, 2e, 3c-3e) or to the axial force required to perfectly flatten the beam (Fig. 2d).

The Euler buckling mode shapes are given by $D \sin \frac{n\pi x}{L}$, where for scaling purposes D is chosen in each case as the maximum displacement of the deformed shape of the FEM results. The Euler buckling loads are found through the well known formula $P_E = \frac{n^2\pi^2 EI}{L^2}$. For the flattened configuration, the axial force corresponds to the force required to shorten the beam to a length equal to the distance between the supports (shortening denoted by

ΔL). The estimate based on linear theory for the axial force at this flattened configuration is given by $N = \frac{EA}{L}\Delta L$, where A is the cross-sectional area. In what follows we will refer to this axial force as 'squash' force.

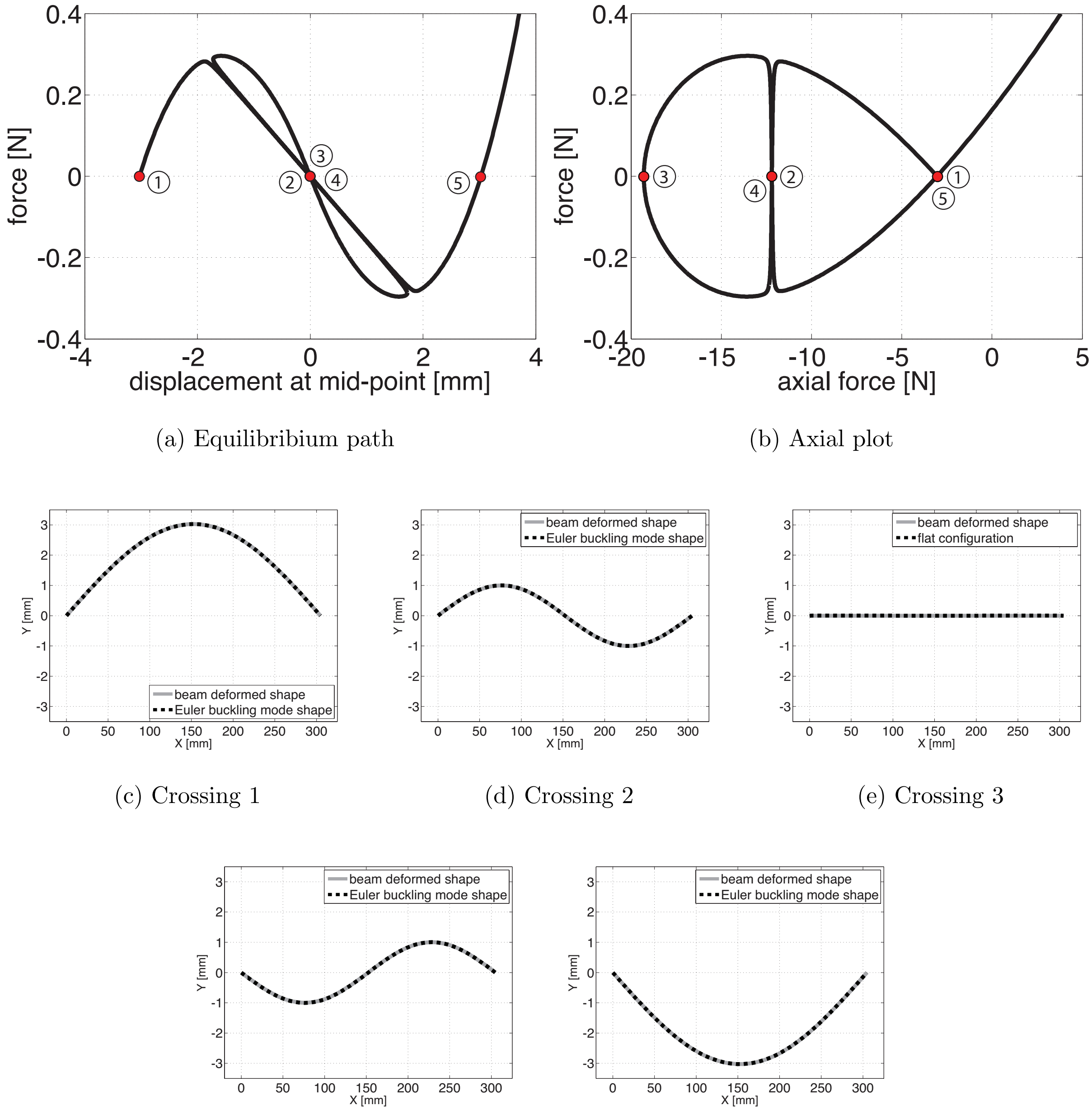

(a) Equilibribium path

(b) Axial plot

(c) Crossing 1

(d) Crossing 2

(e) Crossing 3

(f) Crossing 4

(g) Crossing 5

Figure 4: Equilibrium path and axial plot for beam buckled to rise = 3 mm subject to transverse load applied off-center, and the beam deformed shape at the ZTLCs.

Next we discuss the case where the load is applied off-center. In this case the force-deflection is more interesting, even when the offset is very small. There is only one equilibrium path (Fig. 4a) that passes very near to the original primary and bifurcated branches (approaching it ever more closely with decreasing load offset), effectively stitching them together into one single path.

The equilibrium path starts (approximately) in the (stable) first buckling mode, then passes through the second, then it flattens, after which it passes through the mirror-image second buckling mode and finally the first buckling mode (i.e., the snapped-through configuration) (see Figs. 4c- 4g). In other words, when the load is applied off-center the structure visits all ZTLCs (symmetric and asymmetric).

The axial plot in Fig. 4b shows that at some of the ZTLCs, the curve passes through the same axial force value (in this case crossings labeled 2 and 4 for instance, or the pair 1 and 5). This is also seen in Fig. 5 where the bars show the axial force values at the ZTLCs (black bars) compared to the Euler buckling loads (gray bars). The dashed line corresponds to the axial 'squash' force. The middle black bar corresponds to the maximum axial force at the ZTLCs, and the middle gray bar to the next higher Euler buckling load which is not reached.

The force corresponding to the dashed line in Fig. 5 is the maximum axial force that a beam buckled to a specific rise can encounter. Its significance comes from the ability to predict the highest possible Euler buckling load for a specific geometry (and thereby the number of ZTLCs on the force-deflection curve) by carrying out a simple calculation that only uses information about the shortening ΔL.

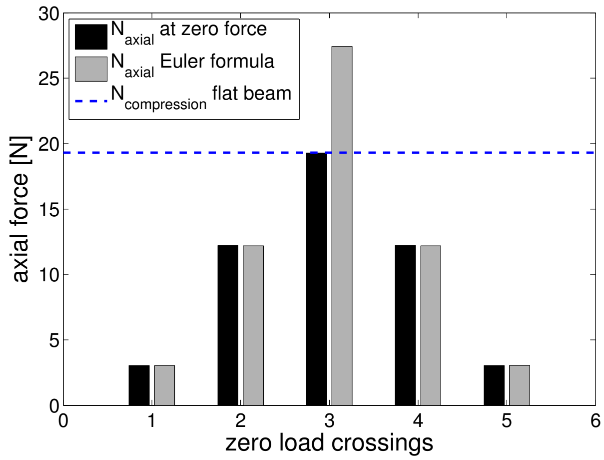

Figure 5: Axial force at the ZTLCs for beam buckled to rise h = 3 mm with off-center transverse load compared to the Euler buckling loads and the force required to flatten the buckled beam.

2.2. Upper bound number of ZTLCs

The number of ZTLCs has an upper bound. We will look next at how the number of ZTLCs changes in order to estimate the upper bound. Consider the initially flat beam from the previous examples, buckled to various rises and subject to off-center transverse load.

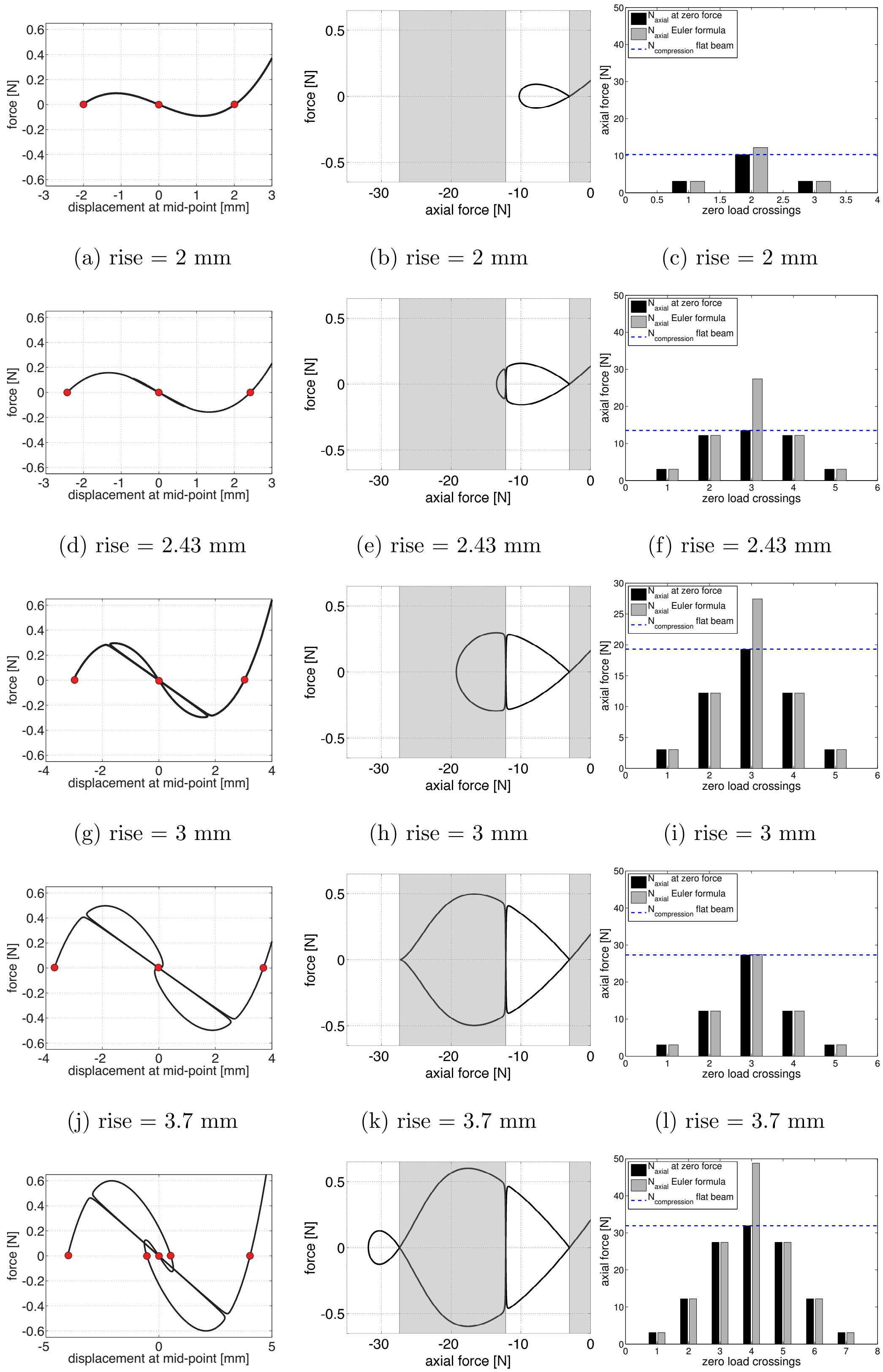

(a) rise = 2 mm (b) rise = 2 mm (c) rise = 2 mm

(d) rise = 2.43 mm (e) rise = 2.43 mm (f) rise = 2.43 mm

(g) rise = 3 mm (h) rise = 3 mm (i) rise = 3 mm

(j) rise = 3.7 mm (k) rise = 3.7 mm (l) rise = 3.7 mm

(m) rise = 4 mm (n) rise = 4 mm (o) rise = 4 mm

Figure 6: Force-deflection curve (left), axial plot (middle), axial force at ZTLCs (right).

The force-deflection curve for the buckling-induced rise $h = 2$ mm is shown in Fig. 6a and the corresponding axial equilibrium plot in Fig. 6b. The three ZTLCs on the force-deflection curve are marked with circles. The two stable equilibria correspond approximately to the first Euler buckling load (two mirror images). On the axial force plot the gray regions correspond to axial force values in the intervals from zero to the first Euler buckling load, and from the second Euler buckling load to the third Euler buckling load. Such a representation allows for an easy comparison between the maximum attainable axial load in the beam and the Euler buckling loads. For this rise the maximum axial force in the beam is below the second Euler buckling load. This implies that the structure will have an axial force at the first crossing equal to the first Euler buckling load, then at the second crossing an axial force value equal to the 'squash' force, finally returning at the third crossing to an axial force equal to the first Euler buckling load (Fig. 6c).

Increasing the buckling rise to $h = 2.43$ mm leads to the force-deflection curve in Fig. 6d. In this case, the force-deflection curve has an additional small loop and five ZTLCs. The axial plot (Fig. 6e) reveals that the maximum axial force value in the beam is higher than the second Euler buckling load, but below the third Euler buckling load. The maximum axial force in the beam and the force necessary to flatten it out compare very well (Fig. 6f). Recall that the analytical expression used to obtain the necessary force to flatten the beam is just a linear approximation.

The size of the loop in the force-deflection curves increases with an increase in the buckling-induced rise as long as the maximum axial force in the beam is below the third Euler buckling load (e.g. see Fig 6d, Fig 6g and Fig 6j).

Further increasing the buckling rise results in axial force in the beam higher than the third Euler buckling load (Fig. 6n). Once the axial force is higher than the third Euler buckling load, another loop appears on the force-deflection curve. Each new Euler buckling load that can be reached represents a seed for a new loop (and two additional ZTLCs) on the transverse force-deflection curve.

The axial plots reveal that at the ZTLCs corresponding to symmetric buckling modes the crossing is shallow, while at the crossings corresponding to asymmetric buckling modes the crossing is steep. The steepness is influenced by the location of the transverse load, decreasing with increase in load offset. Finally, the steepness of the curves indicates that the axial force changes very little throughout asymmetric portions of the equilibrium paths.

The interaction of Euler buckling and snap-through can be thought of through a folding-unfolding analogy. The offset point load initially folds the structure by increasing the spatial wave number (i.e., increasing buckling modes) with each loop before eventually reaching the flat configuration, after which it unfolds the structure through the mirror images of the Euler buckling modes into the snapped-through configuration. For example Fig. 7 shows the details of the path from Fig. 6m. The path starts in the first buckling mode, then the second, third, and finally the flat configuration before traveling backwards through mirror images. Additionally, the given 2D projection of the force-displacement curve is useful in identifying the alternating nature of the asymmetric and symmetric ZTLCs, as the asymmetric crossings have zero mid-span displacement.

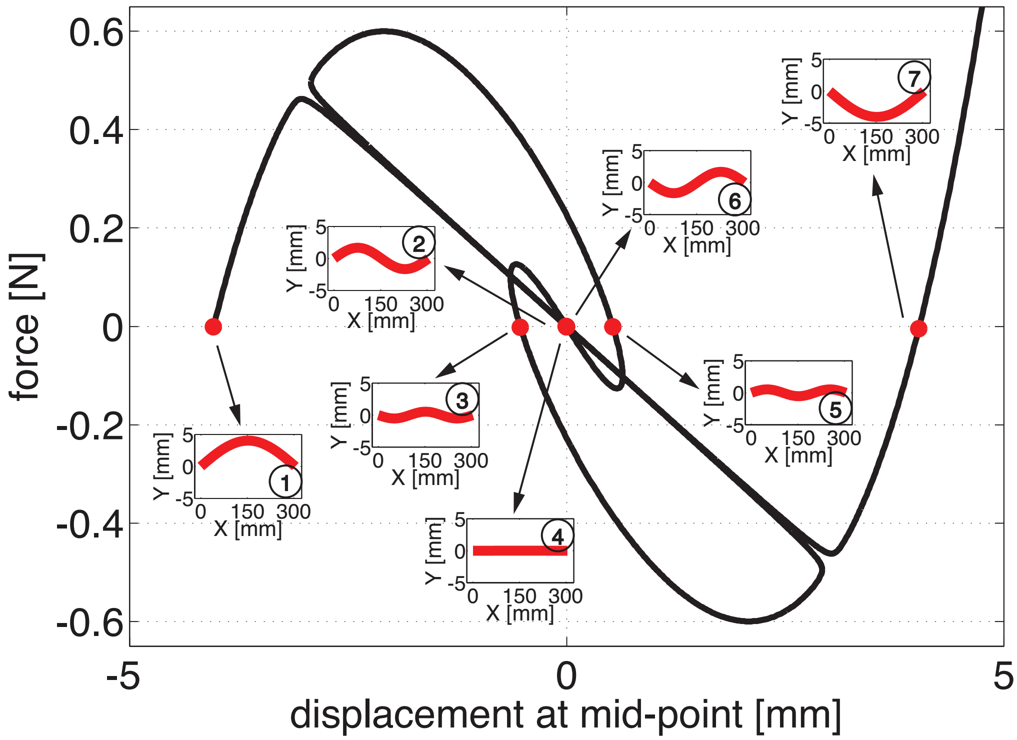

Figure 7: Equilibrium path for beam buckled to rise = 4 mm subject to transverse load applied off-center, and the beam deformed shape at the ZTLCs.

These results show that there is an upper bound on the number of ZTLCs for a buckled beam. This bound depends on the maximum axial load in the buckled beam. The shortening ΔL allows for the rapid calculation of the maximum possible axial force, which facilitates the comparison with the Euler buckling loads. Once the maximum Euler load at the ZTLCs is known, it is straightforward to find the upper bound number of ZTLCs (or the number of equilibrium configurations present without transverse loading). We can write the inequality $\frac{n^2\pi^2 EI}{L^2} \leq EA\frac{\Delta L}{L}$. From this inequality we obtain n_{max} corresponding to the maximum Euler force as $|n_{max}| \leq \sqrt{\frac{AL\Delta L}{\pi^2 I}}$ where n_{max} is the largest integer number satisfying the inequality. If n_{max} satisfies the equality exactly, i.e., $|n_{max}| = \sqrt{\frac{AL\Delta L}{\pi^2 I}}$, then the maximum number of ZTLCs is equal to $2n_{max} - 1$ since each buckling mode is visited twice, except the highest mode, which in this case coincides with the flat configuration and therefore is visited only once. However, if $|n_{max}| < \sqrt{\frac{AL\Delta L}{\pi^2 I}}$, the maximum number of ZTLCs is then $2n_{max}+1$, consisting of the flat configuration and n_{max} buckling modes with each buckling configuration visited twice. Knowing this upper bound is useful, since for a certain rise it provides insight into the degree of instability of the system before running any simulations. Additionally, the maximum number of mode shapes may prove useful in the reduced order modeling or other modal Rayleigh-Ritz type solution methods.

The calculation of ΔL will depend on the type of loading. In the analysis herein, the beams were buckled by applying an end displacement (as an initial step prior to applying transverse load), and therefore ΔL was immediately available as the displacement of the end node. In the case of thermal buckling, the shortening is given by $\Delta L = \alpha L \Delta T$ where α is the coefficient of thermal expansion and ΔT is temperature change. Finally, in the case of initially unstressed curved beams, the ΔL could be determined by calculating the arc-length of the curved beam, and subtracting from it the distance between the supports (although, as stated earlier the results only hold nominally for curved beams).

3. Influence of parameters

In this section we analyze the effects that the geometric parameters and the location and type of the transverse load have on the force-deflection curve and on the number of ZTLCs.

3.1. Effect of rise/thickness

As shown in the previous section, the rise to which a flat beam is buckled influences the force-deflection curve under transverse loading and consequently the number of ZTLCs.

Fig. 8 shows the equilibrium paths as the buckling-induced rise increases. The curves obtained become more complex and the number of ZTLCs increases. It is worth noting that the difficulty in tracing the equilibrium paths also increases with the number of crossings. This is not related to the robustness of the algorithm chosen to trace the equilibrium path, but to the fact that for higher buckling-induced rises the force-deflection curves have more loops that are closer to each other, thus increasing the probability of jumping from one loop to another. The axial plots also become more complex, reflecting the increased number of ZTLCs (Fig. 9).

The relative error (Fig. 10) between the axial load at the ZTLCs and the Euler buckling loads is a metric that reflects the influence of the buckling-induced rise. The relative load error is represented with diamonds for the symmetric modes and with squares for the asymmetric modes. As the rise reduces, the axial load values at the ZTLCs approach the Euler buckling loads. The relative difference between the axial load at the crossing corresponding to the flat configuration and the load to flatten the buckled beam also decreases as the buckling-induced rise approaches the flat configuration. The reason for the larger error for deeper arches is likely due to the simple fact that the equation $EIy^{(IV)} + Py'' = 0$ (with appropriate boundary conditions) from which Euler buckling modes are derived is only accurate for small deformations.

For a specific rise, the relative error of the axial force at the zero crossing configurations decreases as the mode is higher. This is somewhat expected since the load values (and hence the denominators) increase for higher modes, and the magnitude of the deformation decreases, making the linear approximation more accurate. The insensitivity of the axial force to changes in the transverse force over the asymmetric parts of the equilibrium path is a possible explanation for the lower errors of the asymmetric modes. The deformed configurations at the ZTLCs also match the mode shapes very well (the errors $\frac{\int_0^L (y(x)-y_E(x))^2 dx}{L}$ are below 1.5% of the rise for all cases (and usually much lower), where $y(x)$ is the deformed shape of the beam at a ZTLC, and $y_E(x)$ is the Euler buckling mode of a beam with equivalent length).

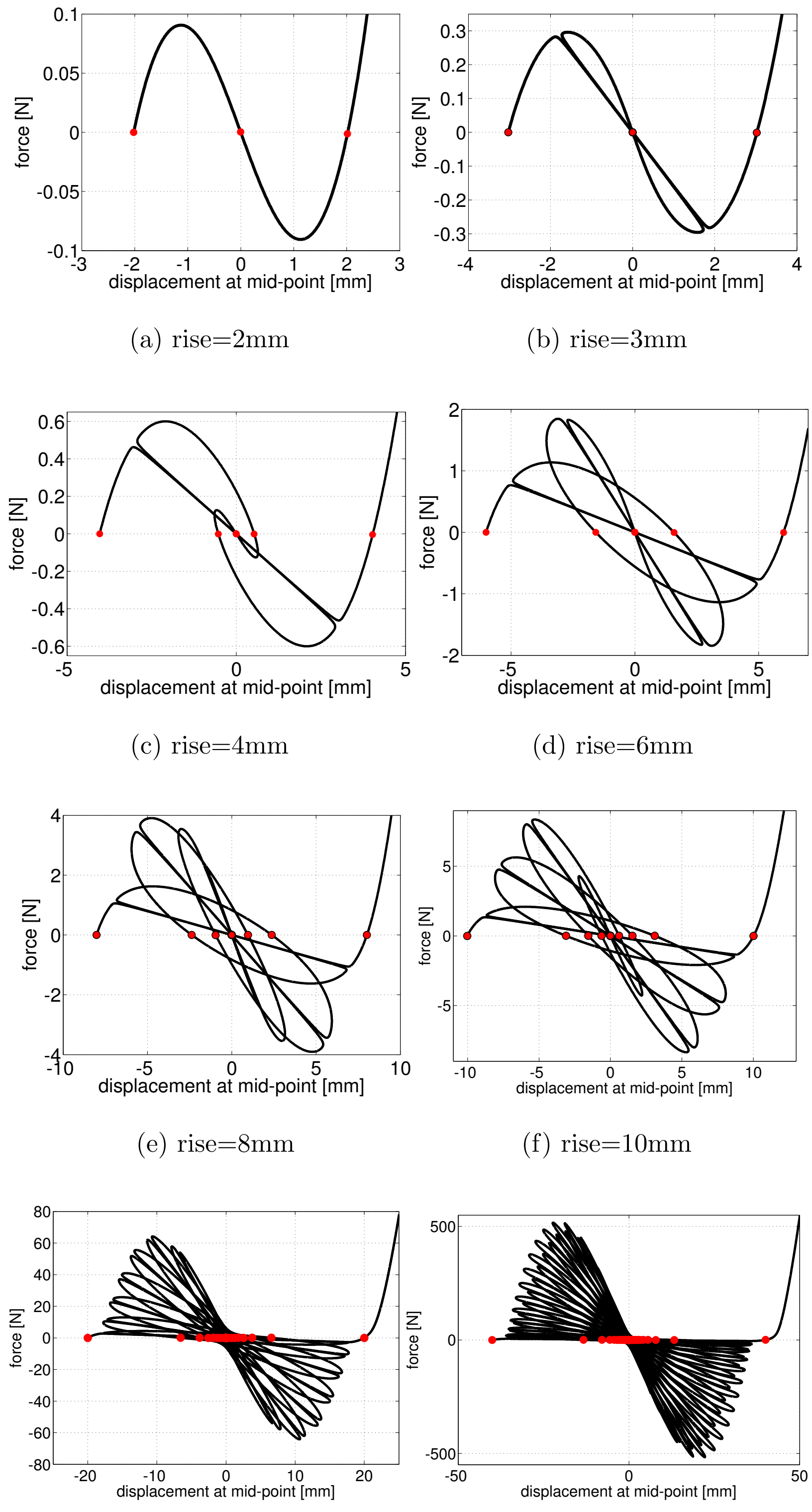

(a) rise=2mm (b) rise=3mm

(c) rise=4mm (d) rise=6mm

(e) rise=8mm (f) rise=10mm

(g) rise=20mm (h) rise=40mm

Figure 8: Equilibrium paths for initially flat buckled beams at different rises subject to transverse off-center load.

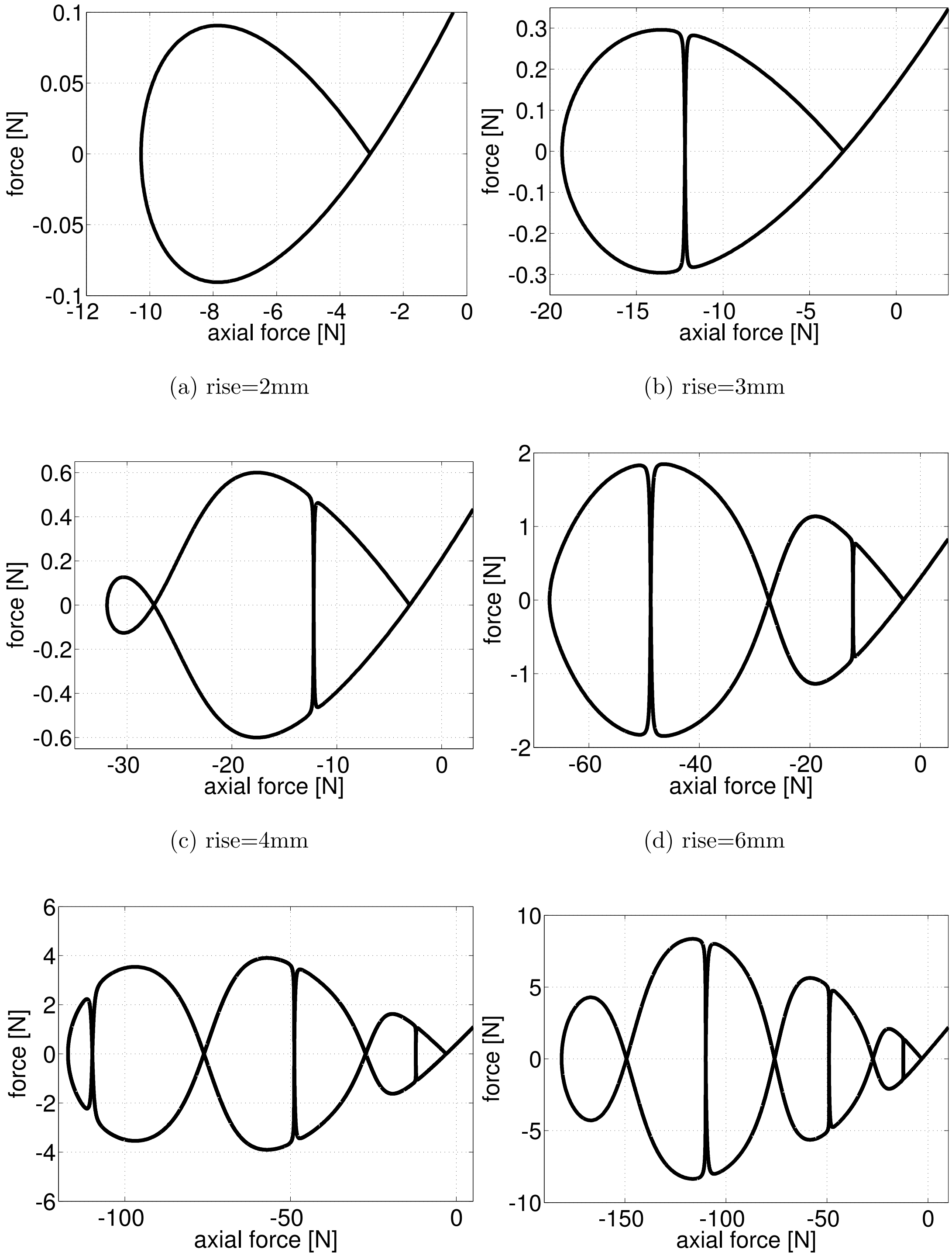

(a) rise=2mm

(b) rise=3mm

(c) rise=4mm

(d) rise=6mm

(e) rise=8mm

(f) rise=10mm

Figure 9: Axial force at each rise level on the equilibrium path for initially flat buckled beams with off-center transverse load for selected rises.

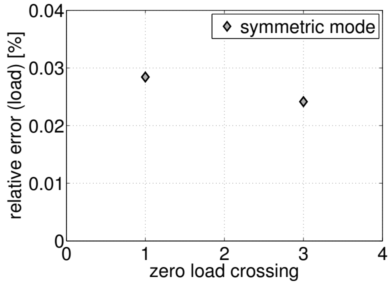

(a) rise=2mm

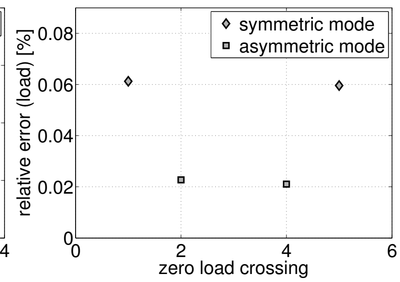

(b) rise=3mm

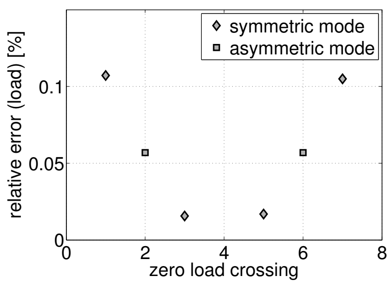

(c) rise=4mm

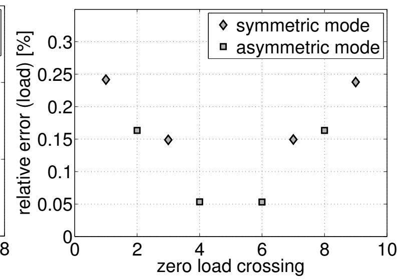

(d) rise=6mm

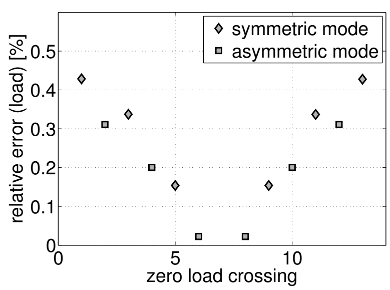

(e) rise=8mm

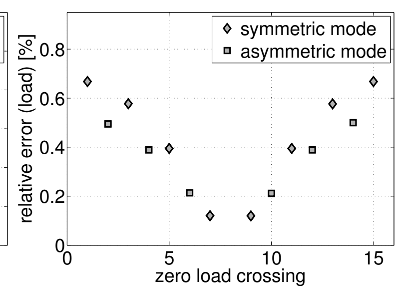

(f) rise=10mm

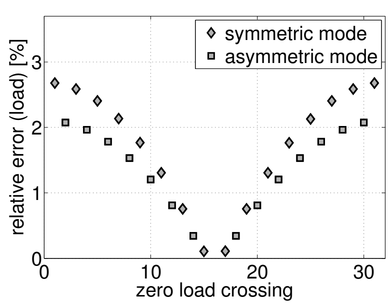

(g) rise=20mm

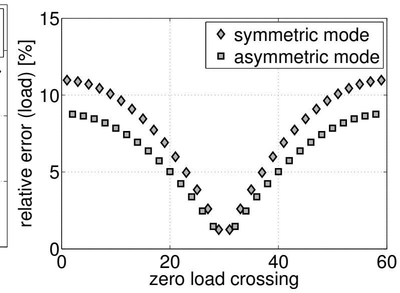

(h) rise=40mm

Figure 10: Relative error between Euler buckling loads and axial force at ZTLCs for initially flat buckled beam with transverse off-center load.

The geometric parameters of the beam influence the force-deflection curve under transverse loading. These parameters are not independent. For the purpose of this study, increasing the axial stiffness (in this particular case changing only the area) or increasing the buckling-induced rise have the same effect on the number of loops in the force-displacement curves [23]. The parameter study was therefore focused only on the variation of the rise.

3.2. Effect of load offset and type

In this paper we have up to this point considered a flat buckled beam that is subjected to a transverse point load applied at the center or slightly off-center. We next investigate how the location of the transverse force affects the force-deflection curve and which of the possible ZTLCs are visited by a particular path-following regime. Figs. 11(a) - 11(c) show the equilibrium paths (transverse force against displacement at the middle point) for a beam buckled to rise h = 8 mm at increasing offset values starting with no load offset, then a very small offset and finally a large offset. Although the force-deflection curves change with the offset, the load offset does not influence the number of ZTLCs, nor does it change the fact that the axial force values at these ZTLCs correspond to the Euler buckling loads. Moreover, regardless of the load offset, all ZTLCs have the same mid-point deflections as indicated by the vertical dashed lines in Fig. 11. The main difference between force-deflection curves for the symmetric mid-point load and for the load with an offset is that for perfectly symmetric load patterns the asymmetric buckling configurations are not captured without branch-switching routines.

Next we examine the influence of the load pattern by applying a transverse distributed load instead of a point load (Figs. 11(d) - 11(e)) and observe that the ZTLCs on the force-deflection curve still have the same mid-point deflections. Therefore, we also conclude that the load type does not influence the location of the crossings. Similarly with the point-load patterns, the asymmetric buckling configurations are not visited when a symmetric distributed load pattern is applied.

The axial force values at the crossings in Figs. 11(b), (c), (e) and (f) compared to the Euler buckling loads corresponding to symmetric and asymmetric mode shapes are shown in Fig. 12. For a center point load (Fig. 11(a)) or a uniformly distributed load (Fig. 11(d)) all the deformed shapes at the ZTLCs are the symmetric mode shapes.

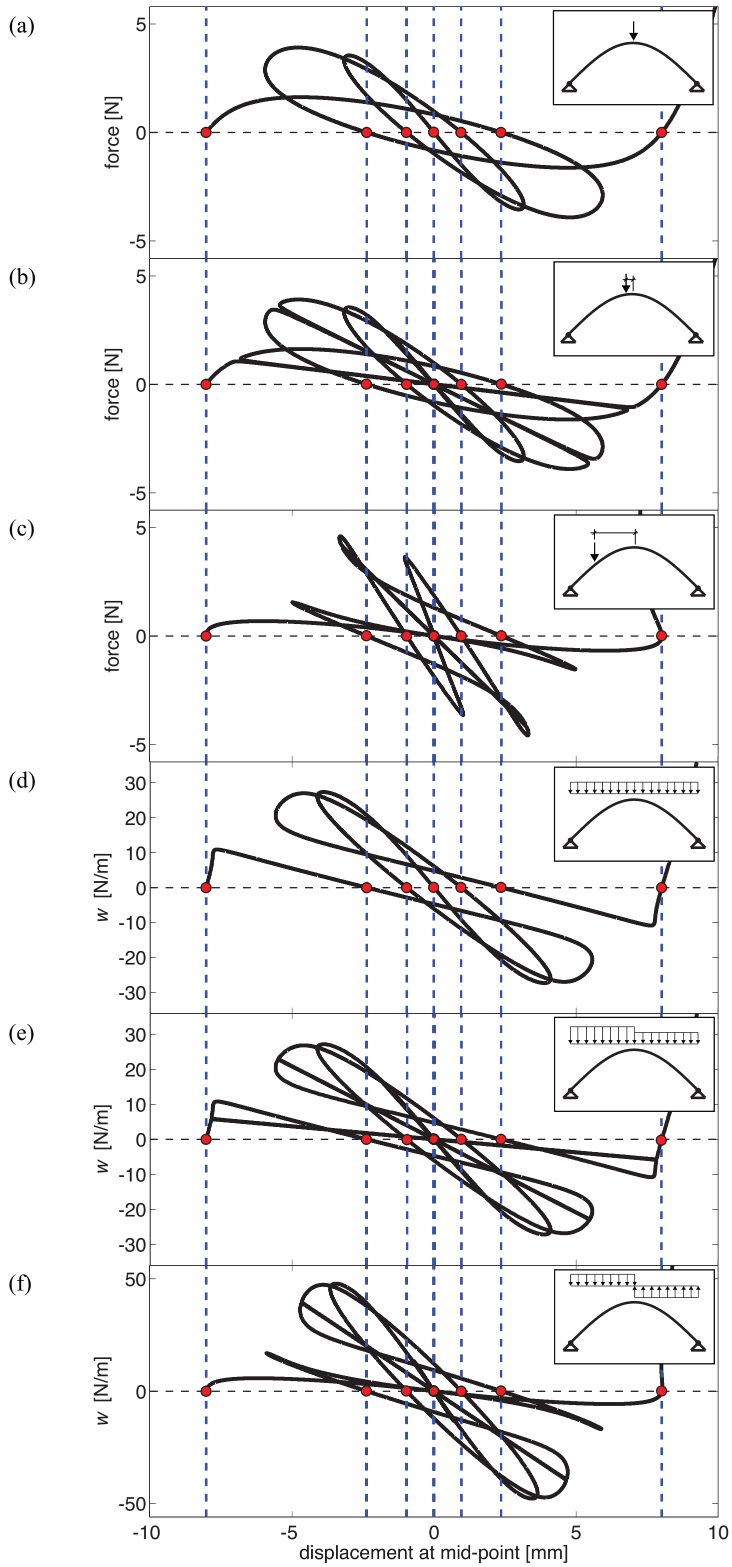

Figure 11: Equilibrium path for beam buckled to rise = 8 mm subject to various force patterns.

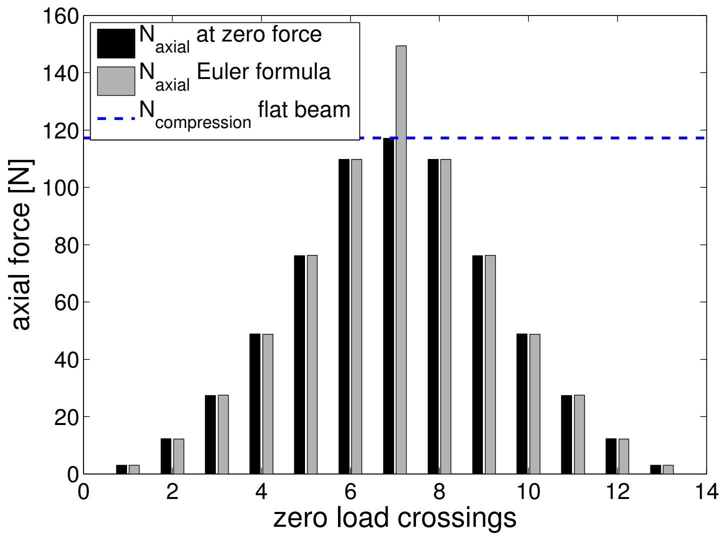

Figure 12: Axial force at ZTLCs compared to the Euler buckling load for beam buckled to rise = 8 mm subject to transverse load (point load or distributed load).

4. Discussions

The results of this work indicate that all of the Euler buckling loads and corresponding mode shapes are connected via the transverse force-displacement path of a beam in the limits: (i) infinitesimal initial rise induced by axial buckling just beyond the first Euler buckling load, and (ii) infinite axial stiffness. Beyond these limits, the Euler buckling relationship provides reasonable estimates of the axial load in the beam at the ZTLCs (with errors of $< 10\%$ for rise-to-span ratios of up to $1/10$ and typically much lower than 1%). Additionally, the method allows for a rapid prediction of the number of "loops" in the force-displacement curve of post-buckled beams by comparing the Euler buckling loads with the axial force of the "flattened" beam.

The ZTLCs of the force-displacement relationship present an interesting window into the potential energy surface of curved and buckled structures. This is because at the

ZTLCs, the pattern of the forcing does not matter as the overall load is zero. The authors conjecture that the ZTLCs visited on the force-deformation paths constitute all of the possible unloaded equilibrium configurations when small asymmetries are induced in the loading. This cannot be guaranteed from the work shown, nor is it guaranteed by the fact that the Euler buckling loads can be used to estimate the number of ZTLCs. This latter point is due to the fact that Euler-Beroulli beam theory is formally correct for linear behavior, and thus arches of very deep rise could potentially exhibit additional stationary points that are fundamentally different than buckling modes (e.g. they could have shapes that do not resemble symmetric or asymmetric buckling modes), with very different bifurcation behavior.

The results presented in the paper are limited to structures with no geometric imperfections. This was done intentionally in order to allow for an exact comparison with the classical Euler buckling. However, in many applications it is difficult to control the dimensions of the beams, and the uncertainties in the geometric parameters in the fabrication process can affect the responses predicted for curved structures. Imperfections were not directly examined, but they are worthy of further study, since they would change the nominal behavior.

Acknowledgement

The Rice University authors greatly appreciate the support from AFOSR under the grant no. FA9550-121-1-0130 and from DOD under the High Performance Computing Modernization Program (HPCMP) grant GS04T09DBC0017.

References

[1] R. H. Plaut, J. C. Hsieh, Oscillations and instability of a shallow-arch under two-frequency excitation, Journal of Sound and Vibration 102 (2) (1985) 189–201.

[2] C. Hsu, On dynamic stability of elastic bodies with prescribed initial conditions, International Journal of Engineering Science 4 (1) (1966) 1–21.

[3] C. Hsu, Equilibrium configurations of a shallow arch of arbitrary shape and their dynamic stability character, International Journal of Non-Linear Mechanics 3 (2) (1968) 113–136.

[4] C. F. Ng, Nonlinear and snap-through responses of curved panels to intense acoustic excitation, Journal of Aircraft 26 (3) (1989) 281–288.

[5] K. D. Murphy, L. N. Virgin, S. A. Rizzi, Experimental snap-through boundaries for acoustically excited, thermally buckled plates, Experimental Mechanics 36 (4) (1996) 312–317.

[6] J. Woo, S. A. Meguid, Nonlinear analysis of functionally graded plates and shallow shells, International Journal of Solids and structures 38 (42) (2001) 7409–7421.

[7] Y. Chandra, R. Wiebe, I. Stanciulescu, L. N. Virgin, S. M. Spottswood, T. G. Eason, Characterizing dynamic transitions associated with snap-through of clamped shallow arches, Journal of Sound and Vibration 332 (22) (2013) 5837–5855.

[8] R. Wiebe, S. M. Spottswood, Co-existing responses and stochastic resonance in post-buckled structures: a combined numerical and experimental study, Journal of Sound and Vibration 333 (19) (2014) 4682–4694.

[9] E. Riks, An incremental approach to the solution of snapping and buckling problems, International Journal of Solids and Structures 15 (7) (1979) 529–551.

[10] M. A. Crisfield, A fast incremental/iterative solution procedure that handles snap-through, Computers & Structures 13 (1) (1981) 55–62.

[11] G. Tzong, R. Jacobs, S. Liguore, Predictive capability for hypersonic structural response and life prediction: Phase 1- identification of knowledge gaps, Tech. rep., Boeing (2010).

[12] B. A. Miller, J. J. McNamara, S. M. Spottswood, A. J. Culler, The impact of flow induced loads on snap-through behavior of acoustically excited, thermally buckled panels, Journal of Sound and Vibration 330 (23) (2011) 5736–5752.

[13] J. S. Han, J. S. Ko, Y. T. Kim, B. M. Kwak, Parametric study and optimization of a micro-optical switch with a laterally driven electromagnetic microactuator, Journal of Micromechanics and Microengineering 12 (6) (2002) 939.

[14] H. M. Ouakad, M. I. Younis, The dynamic behavior of mems arch resonators actuated electrically, International Journal of Non-Linear Mechanics 45 (7) (2010) 704–713.

[15] M. I. Younis, H. M. Ouakad, F. M. Alsaleem, R. Miles, W. Cui, Nonlinear dynamics of mems arches under harmonic electrostatic actuation, Journal of Microelectromechanical Systems 19 (3) (2010) 647–656.

[16] S. Krylov, B. R. Ilic, S. Lulinsky, Bistability of curved microbeams actuated by fringing electrostatic fields, Nonlinear Dynamics 66 (3) (2011) 403.

[17] H. M. Ouakad, M. I. Younis, On using the dynamic snap-through motion of mems initially curved microbeams for filtering applications, Journal of Sound and Vibration 333 (2) (2014) 555–568.

[18] R. Harne, K. Wang, A review of the recent research on vibration energy harvesting via bistable systems, Smart Materials and Structures 22 (2) (2013) 023001.

[19] Y. Zhou, I. Stanciulescu, T. Eason, M. Spottswood, Nonlinear elastic buckling and postbuckling analysis of cylindrical panels, Finite Elements in Analysis and Design 96 (2015) 41–50.

[20] W. Wagner, P. Wriggers, Simple method for the calculation of postcritical branches., Engineering Computations 5 (2) (1988) 103–109.

[21] P. Wriggers, J. Simo, General procedure for the direct computation of turning and bifurcation points, International Journal for Numerical Methods in Engineering 30 (1) (1990) 155–176.

[22] R. L. Taylor, FEAP - Finite Element Analysis Program, University of California, Berkeley, http://www.ce.berkeley.edu/projects/feap/, 2014.

[23] Y. Zhou, W. Chang, I. Stanciulescu, Non-linear stability and remote unconnected equilibria of shallow arches with asymmetric geometric imperfections, International Journal of Non-Linear Mechanics 77 (2015) 1–11.